Hindawi
Journal of Nanomaterials
Volume 2022, Article ID 7012012, 13 pages
https://doi.org/10.1155/2022/7012012

Research Article

Optimization of Synthesis Conditions of β-FeOOH Nanorods towards Antimicrobial Benefits

Fatemeh Mohammadi,[1] **Salme Amiri**,[2] **Esmaeil Mirzaei**,[2] **and Ahmad Gholami**[3]

[1]*Biotechnology Research Center, Shiraz University of Medical Sciences, Shiraz, Iran P.O. Box 71348-14336*
[2]*Department of Medical Nanotechnology, School of Advanced Medical Sciences and Technologies, Shiraz University of Medical Sciences, Shiraz, Iran P.O. Box 71348-14336*
[3]*Pharmaceutical Sciences Research Center, Shiraz University of Medical Sciences, Shiraz, Iran P.O. Box 71348-14336*

Correspondence should be addressed to Ahmad Gholami; gholami@sums.ac.ir

Received 13 September 2021; Revised 14 August 2022; Accepted 24 August 2022; Published 24 September 2022

Academic Editor: P. Davide Cozzoli

FeOOH nanoparticles have recently appealed to wide-ranging applications due to their physicochemical properties and size-tunable synthesis; however, a few studies were performed on the antimicrobial potentials of iron oxyhydroxide nanoparticles. In this regard, we aimed to design various synthesis experiments to optimize the fabrication of β-FeOOH nanorods (NRs) with a desirable size of NRs and high antimicrobial potential. For this purpose, ten experiments were designed by manipulating reaction conditions of the standard hydrolysis method, including the initial concentration of ferric ions, reaction time, reaction temperature, and different concentrations of surfactants of PEI and PEG as process control agents. The structural characteristics of prepared NRs were analyzed using FE-SEM, FTIR, and XRD. The ImageJ software was also used to measure the length, width, and aspect ratio of NRs. Five microbial species, including the Gram-positive and Gram-negative bacteria and fungi species, were applied to investigate the antimicrobial potentials of NRs. The initial concentration of ferric ions revealed a dominant effect in NRs' morphology, though other reaction conditions also played essential roles. The crystal structure of NRs was preserved in all synthesis experiments (β-phase) due to using the same iron salt precursors. The synthesized NRs exhibited dose-dependent antimicrobial activities against all tested microbial species. Additionally, the presence of surfactants exhibited an excellent capability of controlling effects on the size and growth pattern of NR crystals and improving their antimicrobial potentials; PEI could also be more effective on the antimicrobial efficacy of final NRs. Besides, our findings exhibited an inverse correlation between aspect ratio and antimicrobial potentials of β-FeOOH NRs. To sum up, it seems that optimization of synthesis conditions could provide tunable size and structure patterns of β-FeOOH NRs to achieve a promising tool for biomedical applications, particularly in combat with resistant microbial species, though further studies are needed in this regard.

1. Introduction

Antimicrobial resistance, described as a defense mechanism of bacteria or fungi to protect against antimicrobial agents, is one of the ten leading global health issues recommended to track in 2021, based on recent reports by the World Health Organization [1]. It can be associated with over and misuse of conventional antibiotics, the inefficiency of current antimicrobial agents due to low stability and solubility, and possible side effects. Accordingly, new innovative strategies are in high demand to overcome these ever-increasing concerns [2]. For this purpose, novel nanoscale systems for targeted antibiotic drug delivery and some potent antimicrobial nanoparticles (NPs) emerged with great antimicrobial efficacies against various resistant microorganisms [3]. Various nanomaterials have been studied in this regard, like metal NPs, transition metal dichalcogenide nanostructures, and carbon-based nanomaterials, in diverse forms, from single-phase particles to hybrid structures and nanosheets [4–7].

Iron nanoparticles (INPs) are one important and widely used metal NPs due to their unique physicochemical properties, high biocompatibility, low toxicity, and simple synthesis

pathways [8–10]. INPs have received much attention in the last two decades for wide biomedical applications as imaging and therapeutic agents such as magnetic resonance imaging (MRI) and magnetic hyperthermia, gene and drug delivery, biosensor and immunoassay, antimicrobial functions, tissue engineering, cancer therapy, and theranostic approaches [11–14]. Iron oxyhydroxide (FeOOH), as one type of INP, recently appealed to different applications, including water treatment and degradation of organic pollutants due to their potential to generate reactive oxygen species, photocatalyst, solar cell, and ion batteries [15, 16]. According to crystalline structures, it can be found in various nanoscale polymorphs containing goethite (α-FeOOH), akaganeite (β-FeOOH), lepidocrocite (γ-FeOOH), and feroxyhyte (δ-FeOOH) [17]. In recent years, there has been growing interest in optimizing the synthesis of FeOOH NPs, especially in β-phase, to apply in wide applications. The standard synthetic nanostructure of β-FeOOH is nanorods (NRs) which can be achieved by hydrolysis of ferric ions in an aquatic environment and chloride ions [17].

One of the promising applications of β-FeOOH NRs is the capability of converting to magnetic iron oxide NRs. The fabrication of elongated iron oxide NPs directly from iron salts takes complicated procedures due to their preferential cubic orientation in the crystal growth process [18]. This conversion can be implemented by using a reducing agent or calcinating FeOOH NRs in high temperatures above 400°C [19]. Besides, the composites of FeOOH NRs revealed high efficiency in potassium and lithium-ion batteries due to their excellent electrochemical performances, high capacity, and decent cycling stability [20]. Nanoellipsoids of FeOOH were also suggested as food-grade NPs with a good source of ferrous ions in food fortification and supplements [21]. In addition, there is a vast amount of literature on the antimicrobial benefits of FeOOH NPs individually or in a composite of nanostructures incorporated with other elements. Nanocomposites of FeOOH/AlOOH containing iron oxyhydroxide and aluminum oxyhydroxide NPs presented synergistic antimicrobial effects against Gram-positive and Gram-negative bacterial strains without any significant cytotoxicity [22]. Moreover, iron-based nanopillar arrays consisting of Fe_2O_3 and FeOOH NPs exhibited good antimicrobial effects against tested bacteria and fungi strains, which suggested ideal surface disinfection and their ability to grow in various substrates [23]. β-FeOOH NRs have also exhibited high inhibitory effects on biofilm formation, the leading cause of bacterial antibiotic resistance [24].

Despite this interest, no one, as far as we know, has optimized the synthesis of β-FeOOH NRs for antimicrobial applications by considering the influential roles of particle size and concentration of NPs along with preserved morphology. Previous evidence indicated that the initial concentration of iron ions and reaction conditions such as reaction times could significantly effect on characteristics of NRs, particularly the length of rods which, unlike NRs' width, is much tuneable as a result of these changes [25]. Accordingly, we aimed to design different experiments to synthesize β-FeOOH NRs by manipulating reaction conditions of common hydrolysis approaches with different concentrations of iron salt precursors to obtain a potent antimicrobial agent. The antimicrobial evaluation of synthesized NPs was assessed against five microbial species, including the Gram-positive and Gram-negative bacteria and fungi species. In addition, earlier studies highlighted that the presence of additional compounds as surfactants, including polymers such as polyethyleneimine, carbohydrates, salts, acids, and also algal culture supernatant, could improve the fabrication of FeOOH NRs by controlling size, the growth pattern of crystals, and stability [18]. Therefore, we also carried out the synthesis of FeOOH NRs in the presence of two widely used chemical polymers, polyethyleneimine (PEI) and polyethylene glycol (PEG), in deferent concentrations to evaluate their effects on synthesis process and antimicrobial activities of final NRs.

2. Materials and Methods

2.1. Synthesis. FeOOH NRs were generally synthesized by the hydrolysis of ferric ions in aqueous environments, as shown in

$$\mathrm{Fe(III)} + 2\mathrm{H_2O} \longrightarrow \mathrm{FeO(OH)} + 3\mathrm{H^+} \quad (1)$$

A total of ten experiments were designed based on previous studies to optimize the synthesis of β-FeOOH NRs with the highest antimicrobial properties. Parameters considered in designed experiments are as follows, which exhibited significant roles in morphology and size of final NRs: initial concentration of ferric ions; different concentrations of surfactant, PEI, and PEG; and reactions time and temperature. The second compounds containing PEI and PEG were employed in the one-pot method to control the variables of the synthesis process. Firstly, a 40 mL homogeneous ferric chloride solution was prepared with certain concentrations of ferric chloride hexahydrate ($FeCl_3.6H_2O$) and deionized water. The surfactant compounds were employed to control the size of final NPs. So, PEG with final concentrations of 1, 3, and 6% w/v and PEI with concentrations of 0.25, 0.5, and 1.25% w/v were added. Then, the mixture was heated to 80-120°C for 2-12 h under sealed conditions (Table 1). Brownish suspension of synthesized NPs was centrifuged (10000 rpm, 30 min) and rinsed three times with deionized water, and finally, obtained precipitates were dried at 60°C for 24 h and stored at 4°C. During the synthesis process, the color change was observed from light orange to deep brown, confirming the fabrication of β-FeOOH NRs [26].

2.2. Characterizations. FeOOH NRs synthesized with and without surfactants were characterized by field emission scanning electron microscopy (FE-SEM, Mira3, XMU, Germany) and energy-dispersive X-ray spectroscopy detector and mapping (EDX, Mira III, TESCAN) to determine morphology, size distribution, and qualitative analysis; X-ray diffraction (XRD, Siemens D5000, Karlsruhe, Germany) to analyze crystal structures and crystallite size; zeta potential analysis using Zetasizer (Nano ZS-90, Malvern Instruments, UK) to assay surface charge of final NRs; and Fourier

Table 1: Mean size of FeOOH nanorods, length, width, and aspect ratio based from FE-SEM results along with crystallite size of nanorods measured by using XRD data.

Experiment	$FeCl_3.6H_2O$ (gr/mL)	Temperature (°C)	Time (hours)	Surfactant concentration (%w/v)	Length (nm)	Width (nm)	Aspect ratio: length/width	Crystallite size (nm)
1	0.0027	80	10	—	125	34	3.676	23
2	0.0324	80	2	—	120	30	4	18
3	0.05	120	4	—	425	85	5	26
4	0.008	80	12	PEG-1%	216	74	2.919	24
5	0.008	80	10	PEG-3%	165	49	3.367	34
6	0.008	80	2	PEG-3%	129	36	3.58	23
7	0.008	80	10	PEG-6%	154	44	3.5	20
8	0.008	120	4	PEI–0.25%	124	88	1.409	28
9	0.15	120	4	PEI–0.5%	772	103	7.495	21
10	0.15	120	4	PEI–1.25%	661	90	7.34	26

transform infrared spectroscopy (FTIR Spectroscope, Vertex 70, Bruker, Germany) to identify chemical bonds in molecules and assess their chemical properties. The FTIR spectrum of NPs was recorded in the range of 400-4000 cm^{-1} at room temperature using the standard KBr pellet method. The Fe content of each sample was measured by Inductively Coupled Plasma Optical Emission (ICP-OES) spectroscopy (ICP-OES Spectrometer, Perkin Elmer Optima 7300 DV, USA) before treating microorganisms. The ImageJ software, open-source image analysis software, was also used for the measurement of length, width, and aspect ratio of NRs.

2.3. Antimicrobial Assay. The antimicrobial potential of as-prepared β-FeOOH NRs was assessed by microdilution methods, based on the clinical and laboratory standard institute (CLSI, 2019), against Gram-positive and Gram-negative bacterial species and a common fungal pathogen of humans. For this purpose, *Staphylococcus aureus* (*S. aureus*) PTCC 1112, *Enterococcus faecalis* (*E. faecalis*) PTCC 1778, *Escherichia coli* (*E. coli*) PTCC 1399, *Salmonella typhi* (*S. typhi*) PTCC 1609, and fungal species of *Candida albicans* (*C. albicans*) PTCC 5027 were purchased from Persian type culture collection center. Bacterial species were cultured in BHI media at 37°C with 200 rpm agitation, and *C. albicans* was cultured in an RPMI culture medium. The microdilution method was applied to achieve the minimum inhibitory concentration MIC of NRs and quantitatively report their antimicrobial potentials against microbial strains. The MIC value was considered the lowest concentration of NRs able to inhibit 90% of microbial growth after overnight incubation.

10 μL of prepared bacterial suspension containing about 5×10^6 CFU/mL inoculated to the wells of a 96-well microplate containing 90 μL medium with the concentration of 500, 250, 125, 62.5, 31.25, 16.12, 8, and 4 μg/mL of each synthesized NRs. After 24 hours of incubation of microplates at 37°C, the optical density of all wells was measured by a microplate reader (PowerWave XS2, BioTek Instruments Inc., US) at 600 nm. Control groups were defined as wells containing medium with the same microbial inoculation without any NRs and blank groups containing medium without microbial inoculation or NRs.

3. Results and Discussion

Nanostructures of akaganeite are generally found in elongated orientations such as rods or ellipsoids, which can be formed in iron- and chloride-rich environments and heating to at least 80°C. In contrast, this hydrothermal reaction prolongs at least six months at room temperature [27]. Through the akaganeite synthesis process, as Fe salts dissolve in water, Fe^{3+} ions will make a complex with water molecules and from $[Fe(H_2O)_6]^{3+}$. Then, the synthesis process is continued by hydrolysis reaction in two steps, release of protons from water molecules and formed double octahedral units via Fe −OH−Fe bonds, which can interact strongly or weakly with various anions, and form various morphology and size of FeOOH nanorods in the polymerization step [28]. Thus, the type of anions of ferric salt plays a determinative role in the final size and crystallization of the products. Yue et al. described the synthesis of β-FeOOH NPs from different iron salts in an experimental and theoretical study and suggested $FeCl_3$ for achieving β-FeOOH NRs [29]. According to their evidence, firstly, hydrothermal reaction arranges FeO_6 octahedral units to form FeOOH seeds, double octahedral units, and finally lattices.

During the growth process, chloride ions are adsorbed on the surface of FeOOH lattices due to high electronegativity and direct the growth of NPs through elongated structures by strong interactions (Figure 1). This study highlighted the significant effects of various anions of ferric salts on the morphology and size of obtained FeOOH NPs. $FeCl_3$ salt leads to the formation of FeOOH NRs in the β phase. However, other salts of iron provide different morphology of FeOOH NPs. $Fe(NO_3)_3$ helps the synthesis of spherical goethite NPs (α-FeOOH), and the $Fe_2(SO4)_3$ salt leads to produce amorphous FeOOH NPs with irregular morphology [29].

There is a considerable amount of optimization studies on NP synthesis using almost the same synthesis protocols, obtaining distinct characteristics and properties, including size, morphology, crystallinity, and biological activities. It has been performed just with some simple and facile changes in reaction conditions or precursors without any remarkable

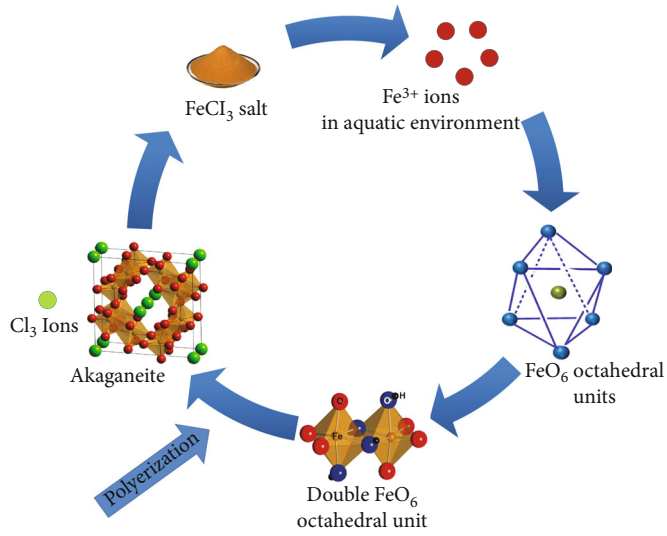

Figure 1: Schematic diagram illustrating the synthesis mechanism of β-FeOOH nanorod structures from ferric ions in the aquatic environment.

modifications in the protocol of synthesis. Sayed and Polshettiwar reported the synthesis of iron oxide nanoparticles in six different morphologies denoted as follows, based on the same protocols with simply changing precursor iron salts: distorted, nanocubes, porous spheres, and self-oriented flower shapes [30]. Moreover, Moradpoor et al. described nine different synthesis experiments of cobalt oxide NPs to obtain an optimal antibacterial agent. In this case, the same protocol was applied in experiments with changes in the reaction conditions, such as stirring time and concentrations of precursors containing cobalt salts and reducing agents [31].

In this work, we aimed to optimize the fabrication of β-FeOOH NRs to achieve the desired size along with the high potent antimicrobial activity. Although FeOOH NPs can be formed in rod-like morphologies without using addictive compounds, however, appropriate surfactants can facilitate the synthetic process and control the growth pattern of crystals in uniform size and shape [32]. Accordingly, we applied PEG and PEI polymers as process control agents to the one-pot synthesis of β-FeOOH NRs and four Gram-positive and Gram-negative bacterial strains, including S. aureus, *E. faecalis*, *E. coli*, and *S. typhi*, and one of the pathogenic fungal species, *C. albicans*, to find the best antimicrobial potent NR of as-prepared NPs.

3.1. Characterizations. Figure 2 displays the FE-SEM micrograph of synthesized NPs achieved from designed experiments. All NPs exhibited elongated and rod-like morphology with almost good monodispersity. The mean size and aspect ratio of NRs were evaluated by size measurement of at least 100 NPs selected at random per condition by the ImageJ software. Table 1 illustrates the measured length and width mean sizes and aspect ratio per experiment individually.

As indicated in previous literature, the concentration of ferric salts plays a defining role in the synthesis of β-FeOOH NPs by controlling the growth of nanocrystals. Increasing the concentration of ferric ions leads to an increase in the length of NRs without significant width change and subsequently elevated aspect ratio since a higher concentration of ferric salts provides more ferric precursor along with more acidic pH, facilitating parameters in the hydrolysis process and further growth of NRs [28, 33]. In this regard, we also found that increasing the concentration of ferric ions raises the length of NRs without a significant change in aspect ratio (Table 1). Moreover, surfactants are considered a decisive factor in NR synthesis by tuning the morphology [34, 35]. As shown in the results, more concentration of PEG leads to a decreased size of final NRs without significant change in aspect ratio, 3.5 compared to 2.9 (Exp. 7 to Exp. 4). Kasparis et al. also confirmed the significant role of surfactants on the morphology of FeOOH nanorods. A high concentration of PEI revealed significant decreases in NPs with well-preserved crystal structure and aspect ratio [18]. However, unlike the expected effects of surfactants, the increase of PEI concentrations in Exp. 9 and 10 made their particle size larger than Exp. 8 and remarkably changed in aspect ratio (7.34 compared to 1.41). This reveals the dominant role of higher ferric ions concentration in synthesis reaction that minimizes the surfactant effects, increasing the length of NRs and, after that, increasing the aspect ratio.

Nevertheless, reductive effects of PEI on the mean size of NPs can be observed in NPs obtained from Exp. 10 compared to Exp. 9. All of the synthesis conditions were similar in the two experiments except for the increased concentration of PEI surfactant in Exp. 10, providing a smaller size of NPs with a similar aspect ratio. Additionally, we found that although Exp. 7 was carried out in the presence of a higher concentration of PEG compared to Exp. 6, however, size of NPs increased without a change in aspect ratio. It can result from an increased time reaction of up to 10 hours that could improve the growth of crystals and provide a larger size of NRs. Notably, the aspect ratio did not change significantly in this experiment, and the size change was limited due to the tuning effects of surfactants.

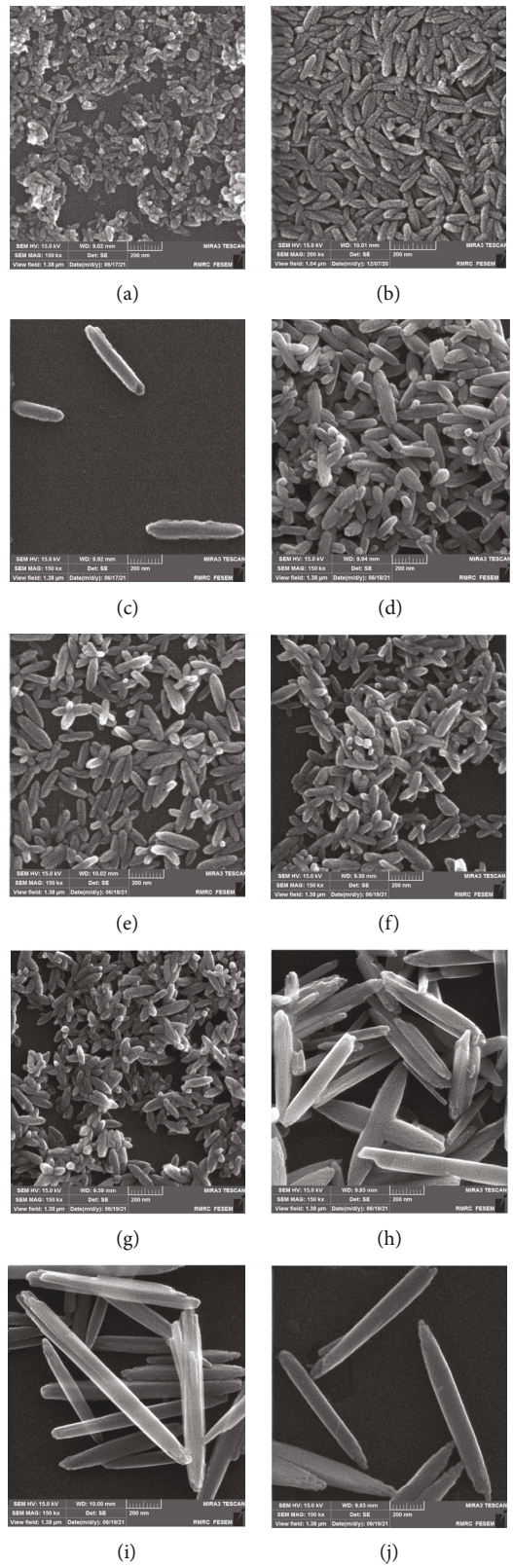

Figure 2: FE-SEM micrographs of the β-FeOOH nanorods synthesized by various synthesis experiments: (a–j) Exp. 1-10, respectively.

As proposed in previous studies, the evidence we found highlights the influential role of surfactants like PEG and PEI in controlling the particle size and improving the size distribution of final β-FeOOH NRs during fabrication. PEG molecules favor the fabrication of smaller sizes of β-FeOOH NRs, as suggested by Wei et al. The possible

Table 2: Effects of various synthesis parameters on the structural properties of prepared β-FeOOH nanorods.

Structural properties of final NPs	Kind of Fe salts (anions)	Fe salt concentration	Reaction time	Surfactant concentration
Morphology (size)	*	*	*	*
Aspect ratio	*	*	—	—
Crystal structure	*	—	—	—

*Dependent-Independent.

mechanisms that PEG surfactant firmly coordinated with ferric ions (Fe^{3+}) through OH functional groups were proposed to explain this effect, which prevents nuclei aggregation and subsequently achieves the smaller size of β-FeOOH NRs. Furthermore, PEG surfactant avoids the aggregation of final synthesized NRs and maintains the size and morphology [34].

In addition, in earlier investigations, the role of PEI polymer in improving the morphology of metal oxide NRs and reducing their diameters and length has been argued in detail. For this purpose, PEI as a cation surfactant was suggested to limit the lateral growth of NRs remarkably by adsorbing on the negatively charged lateral facets of NRs during the synthesis process owing to electrostatic interaction. Moreover, amino groups of this surfactant coordinated with NRs, which led to obtaining NRs with smaller diameters than synthesized NPs without surfactants [36]. Besides, PEI was argued to be the controlling agent of length and width of β-FeOOH NRs by Mohapatra et al. The adsorption of PEI molecules on the lateral plan of NRs was suggested for the mechanism of this action [37].

Reaction time is one of the other factors that can affect the morphology of FeOOH NRs. Kasparis et al. reported that the increasing reaction time from 30 min to 4 hours made larger NRs without effects on the aspect ratio [18]. In this study, we also found that NRs achieved larger size with preserved aspect ratio by extending reaction times from 2 to 10 h in the presence of a consistent concentration of PEG and ferric ions (Exp. 5 compared to Exp. 6), even though this size change was limited due to presence of surfactant. In addition, while the reaction time of Exp. 1 was more than Exp. 3, obtained NPs did not show a larger size and even revealed a smaller size and aspect ratio. These findings confirm the dominant effect of ferric ions concentration, as the concentration of iron salts applied more in Exp. 3.

Our findings appeared well substantiated by previous studies on effective parameters for synthesis reactions containing ferric ion concentration, presence of surfactant, and reaction time (Table 2). Findings suggest that ferric ion concentration is the dominant factor in the morphology of NRs. Also, surfactants such as PEI and PEG can be good candidates to tune the size and aspect ratio of β-FeOOH NRs efficiently. The aspect ratio is independent of all factors except ferric ion concentrations. Moreover, in the consistence of other synthesis parameters, time reactions can cause the overgrowth of NRs; therefore, it should also be considered to tune NR morphology. Furthermore, EDX spectroscopy was performed for qualitative analysis and chemical characterization of β-FeOOH NRs prepared with and without the presence of surfactants, as revealed in Figure 3. As shown in the results, a desirable percentage of Fe and O was obtained in all NRs, which confirms the successful formation of β-FeOOH NRs. Moreover, the contents of C, N, and O in the results related to NRs obtained from synthetic EXP 4-10 indicated the surface functionalization of NRs by PEG and PEI.

The FTIR spectrum of prepared NRs is exhibited in Figure 4. According to previous studies, specific characteristic peaks should be assessed to analyze and confirm the appropriate synthesis of FeOOH NPs chemically. The absorption peaks in the 300 to 700 cm^{-1} have frequently been assigned to fundamental vibrational bands of inorganic ions [3]. FeO_6 octahedral units of β-FeOOH NRs are identified by characteristic peaks of two prominent vibration bands, FeO and OH groups. The vibration of FeO groups of octahedral units was observed as Fe−O bending vibrations at about 400 cm^{-1} and Fe−O stretching vibrations containing symmetrical stretching bands from 435 to 495 cm^{-1} and asymmetrical stretching bands at 647 to 700 cm^{-1} [28, 38, 39]. As shown in Figure 4, the characteristic absorption peaks related to Fe−O bands of octahedral sites are perceptible between 400 and 700 cm^{-1} in all sample graphs. In addition, structural OH bands as Fe-OH in the octahedral site are recognized by bending vibration at ~818 cm^{-1}. Also, O-H…O bending vibration in Fe−O−OH bands is reported between 840 and 850 cm-^{1} [28, 39]. The FTIR spectrum of all samples represents the prominent absorption peaks in the range of 820-850 cm^{-1}, confirming the existence of structural OH groups in octahedral units of FeOOH NRs. In line with former findings, the stretching and bending vibrational bands of surface hydroxyl groups were found at a range of about 3390-3490 and 1620-1650 cm^{-1}, respectively, corresponding to possible adsorbed water molecules in FeOOH NPs [14, 38]. The additional bands detected in the region of 1550–1350 cm^{-1} and 2850–3000 cm^{-1} are assigned to artefacts of the preparation or organic contaminants. However, some evidence considered the absorption bands located in 1350 to 1490 cm^{-1} peculiar to β-FeOOH NPs and convenient to differentiate it from other phases [39]. Additionally, surface functionalization of NRs with PEG and PEI surfactants could be confirmed by the characteristic peaks related to C–H and N-H vibration of hydrocarbon chains and the amine groups of the polymer structures in the FTIR spectrum of NRs (Figure 4). The corresponding peaks of the stretching and bending vibration of C-H bond appeared at 2800–3000 cm^{-1} and 1300-1500 cm^{-1}, respectively [40–43], as our findings also illustrated these absorption ranges as small peaks (Figures 4(b) and 4(c)). Moreover, previous findings reported that the absorption peak range of 1500-1650 cm^{-1} and 3000-3400 cm^{-1} were ascribed to N-H

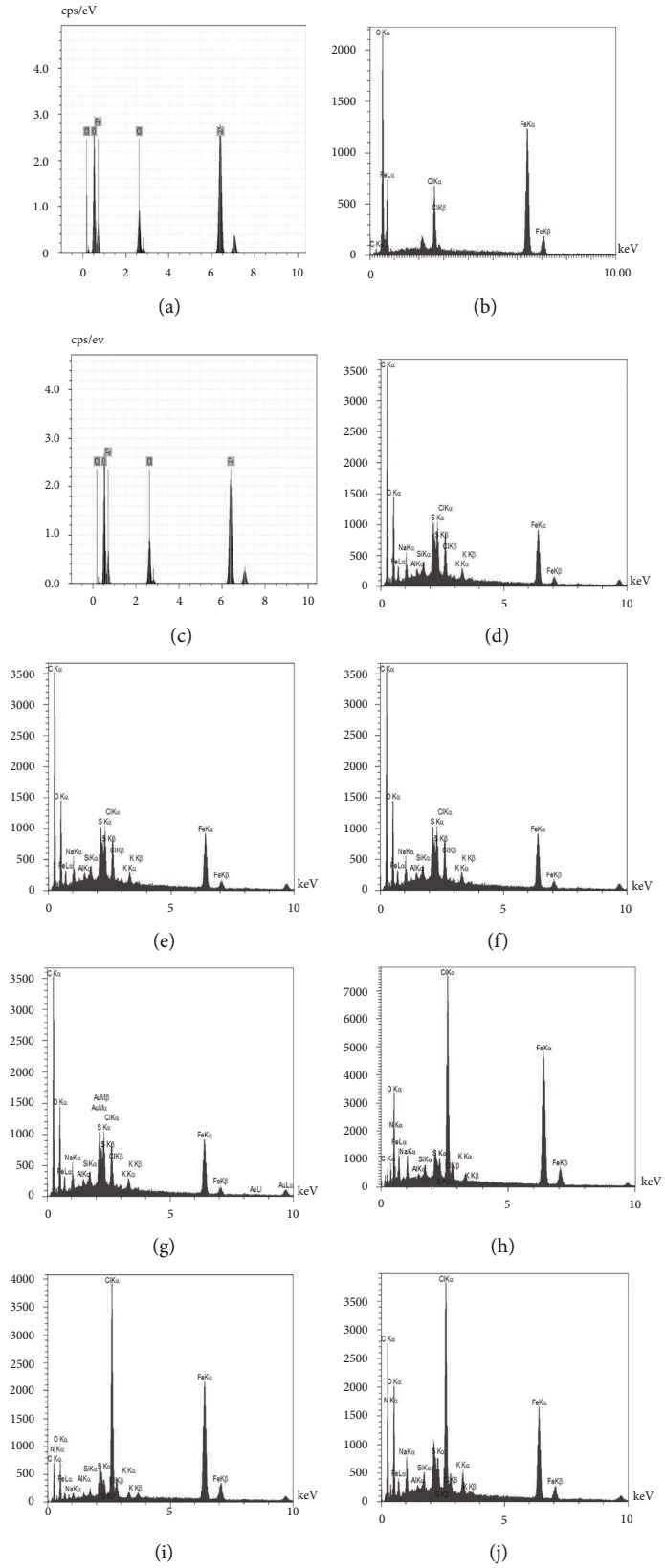

Figure 3: EDX pattern of β-FeOOH nanorods synthesized by various synthesis experiments. (a–c) Exp. 1-3, NRs without surface functionalization. (d–g) Exp. 4-7, NRs with PEG surface functionalization. (h–j) Exp. 8-10, NRs with PEI surface functionalization.

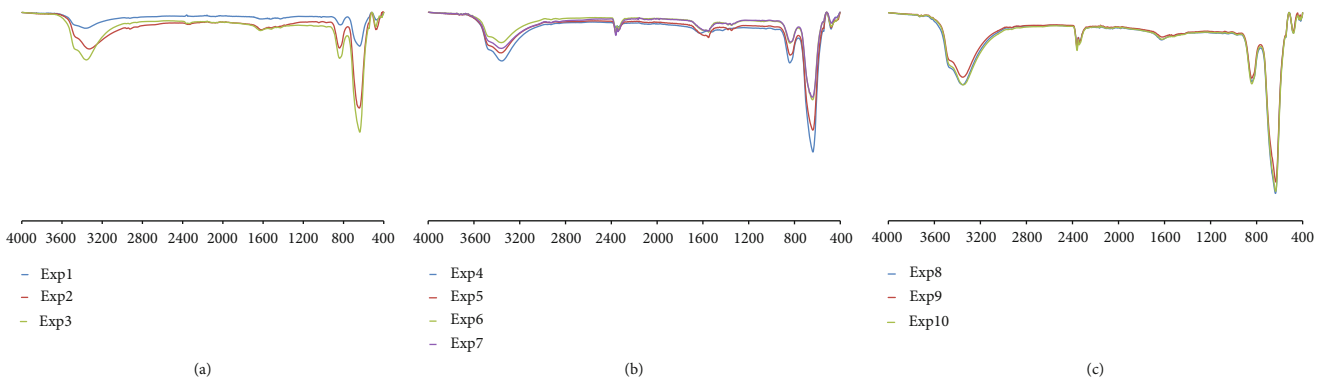

FIGURE 4: FTIR spectra of the β-FeOOH nanorods prepared by various synthesis experiments. (a) Exp. 1-3, NRs without surface functionalization. (b) Exp. 4-7, NRs with PEG surface functionalization. (c) Exp. 8-10, NRs with PEI surface functionalization.

bending and stretching vibration region related to the amine groups of PEI molecules [44–46], which are illustrated in Figure 4(c) as a broad peak in the region of 3000 to 3500 cm^{-1} that seems to be overlapped with the peaks of O–H stretching vibrations.

The XRD patterns FeOOH NRs as prepared through different designed experiments of the one-pot hydrothermal method are provided in Figure 5. All of the diffraction peaks were consistent well with the typical values of β-FeOOH NR pattern based on the Joint Committee of Powder Diffraction Standards (JCPDS) database (reference code: 00-034-1266), related to the tetragonal body-centered crystal structure of β-FeOOH with lattice parameters: $a = b = 10.535$ Å, $c = 3.03$ Å, and $V = 336.29$ $Å^3$. As shown in Figure 5, all of the reflection peaks were well indexed to a similar tetragonal phase of β-FeOOH and in line with previous reports [47]; the crystal structure of β-FeOOH NRs is independent of synthesis parameters manipulated in this work, including ferric ion concentration, surfactant concentration (PEG and PEI), temperature, and time reaction.

In this regard, a similar experiment reported that the presence and concentration of size-controlling agents such as PEI and different HCl molarities have no significant impacts on the crystal structure of prepared β-FeOOH NRs [18, 48]. Similar results were also confirmed that the β-FeOOH crystals are independent of the concentration of ferric ions in hydrolysis synthesis [28, 33]. Moreover, Parameshwari et al. reported that a sufficient amount of dextrose as a chelating agent is required to acquire a stable and single phase of β-FeOOH in the coprecipitation method. The coexistence of the secondary phase of FeOOH occurred in low concentrations of dextrose [38].

In addition, in this study, the crystallite size of NRs was measured using XRD data, which revealed a narrow-range difference between all samples, 18-34 nm. It implies that various synthesis conditions could not significantly impact the crystallite size of NRs, despite their remarkable impacts on the length and width of final NRs (Table 1). Before assessing the antimicrobial effects of synthesized NRs, each sample's surface charge and iron concentration were determined by zeta potential analysis and ICP-OES spectroscopy, as shown in Table 3. The results noticeably indicated the positive surface charge of β-FeOOH NRs prepared in the presence of PEI surfactant (Exp. 8-10), which increased 15.5 ± 5.8 to 62.9 ± 0.6 due to the rise of PEI concentration from 0.25-1.25% w/v, while zeta potential measurement showed the negative surface charge of β-FeOOH NRs synthesized in the presence of PEG or without surfactant agents (Exp. 1-7). Consistent with previous evidence, this positive surface charge owning to surface modification of NPs could play a significant role in their biological behaviors, particularly antimicrobial activities [49, 50]. Moreover, according to ICP data, the concentration of Fe was found within a narrow range of concentration in all samples, between 212.68 and 307.38 μg/mL (Table 3). The impact of this difference between the iron content of samples seems negligible in evaluating NRs' antimicrobial properties.

3.2. Antimicrobial Assay. Antibacterial and antifungal activities of prepared β-FeOOH NRs synthesized with and without surfactants were evaluated by microdilution against five pathogenic microorganism species, including *S. aureus*, *E. faecalis*, *E. coli*, *S. typhi*, and *C. albicans*. Figure 6 represents the viability percentage of microorganisms treated by 500, 250, 125, 62.5, 31.25, 16.12, 8, and 4 μg/mL of each synthesized NRs. All NRs exhibited dose-dependently inhibitory effects on microbial growth; higher concentrations led to more growth inhibition, as shown in the results. According to MIC value (Table 4), Gram-negative species demonstrated more susceptibility than Gram-positive bacterial species; *S. typhi* showed the most and *S. aureus* and *E. faecalis* the least susceptibility to NRs. Gram-positive bacteria such as staphylococci, enterococci, and pneumococci are currently known as pathogens of great concern due to their intrinsic virulence inducing various infections and exceptionally high multidrug resistance, which should be addressed before long [51]. Based on the results, Synthesized NRs could inhibit the growth of *S. aureus* and *E. faecalis*, mostly just in high concentrations.

The impacts of surfactant presence on the antimicrobial properties of final NRs were evaluated by comparing the results of Exp. 1, 6, and 8, NRs with fairly similar length sizes that were obtained, respectively, in the absence of any surfactants and in the presence of PEG and PEI. NRs synthesized in the absence of surfactants exhibited the least antimicrobial effects on all tested microbial species; however, surfactant

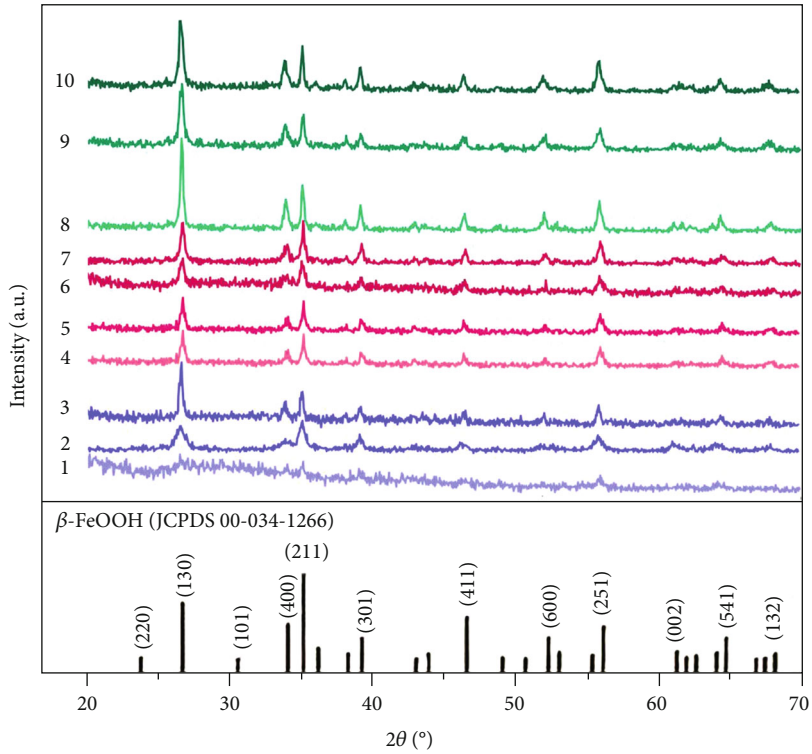

Figure 5: XRD patterns of the β-FeOOH nanorods synthesized by various synthesis experiments (1–10) and the standard pattern of akaganeite (β-FeOOH) crystals (JCPDS 00-034-1266).

Table 3: Zeta potential values and ICP-OES analysis results of β-FeOOH nanorods obtained from synthetic Exp. 1-10, with and without the presence of surfactants.

Experiment	Surfactants (w/v)	Zeta potential (mV)	Charge	Final content (μg/mL)
1	—	−5.21.4 ± 1.4	Negative	307.38
2	—	−14.1 ± 2.2	Negative	278.38
3	—	−21.2 ± 2.3	Negative	212.68
4	PEG-1%	−27.4 ± 2.0	Negative	242.02
5	PEG-3%	−41.3 ± 0.3	Negative	240.89
6	PEG-3%	−45.3 ± 0.5	Negative	286.84
7	PEG-6%	−54.2 ± 0.4	Negative	235.67
8	PEI–0.25%	15.5 ± 5.8	Positive	257.845
9	PEI–0.5%	56.3 ± 0.2	Positive	270.65
10	PEI–1.25%	62.9 ± 0.6	Positive	252.54

presence PEI in the synthesis process contributed to achieving NRs with remarkably higher potential of antimicrobial activities: Exp. 8> > Exp. 6 > Exp. 1. PEG and PEI are synthetic polymers considered individually antimicrobial agents and act as microbicidal enhancers in antibiotics, especially against resistant bacterial species [52, 53]. Coating of polycationic polymers such as PEI exhibited highly electrostatically interact with the bacterial membrane due to its negatively charged and result in increased membrane permeability, penetration of conjugated materials to bacteria cells, and finally disturbing cell structure and raising cell death [53]. Grafted PEG coating was also found to be contributed to the bactericidal effects of nanocomposites, particularly against resistant bacteria species, by providing a hydrophilic environment to avoid bacterial inhesion and biofilm formation, which also gives the conjugated nanomaterials offer additional bactericidal effects [54]. Thus, the higher antibacterial action of PEG and PEI conjugated synthesized NRs could be assigned to polymers' instinct antimicrobial properties as well as synergistic effects of these polymers.

On the other hand, the impact of aspect ratio on the antibacterial efficacy of NRs cannot be ignored. The aspect ratio is considered a critical factor in the cellular uptake of rod-like NPs [55]. NP uptake by microorganisms is related to physicochemical properties, particle orientation, and membrane properties. Moreover, the surface active agents can be involved in particle characterization changes such as aspect ratio and interactions with biological samples, membrane wrapping, and subsequent internalization [56]. The higher aspect ratio of NRs is less favored for microbial particle uptake and antimicrobial efficacy.

In the present case, Exp. 1, 6, and 8 displayed the aspect ratios of 3.676, 3.58, and 1.409, respectively. Exp. 8 obtained a lower aspect ratio due to different synthesis conditions and the presence of PEI. Based on the results, these samples exhibited remarkably more antimicrobial impacts on all microbial species, which along with PEI antimicrobial activities; it could be related to the decreased aspect ratio of these

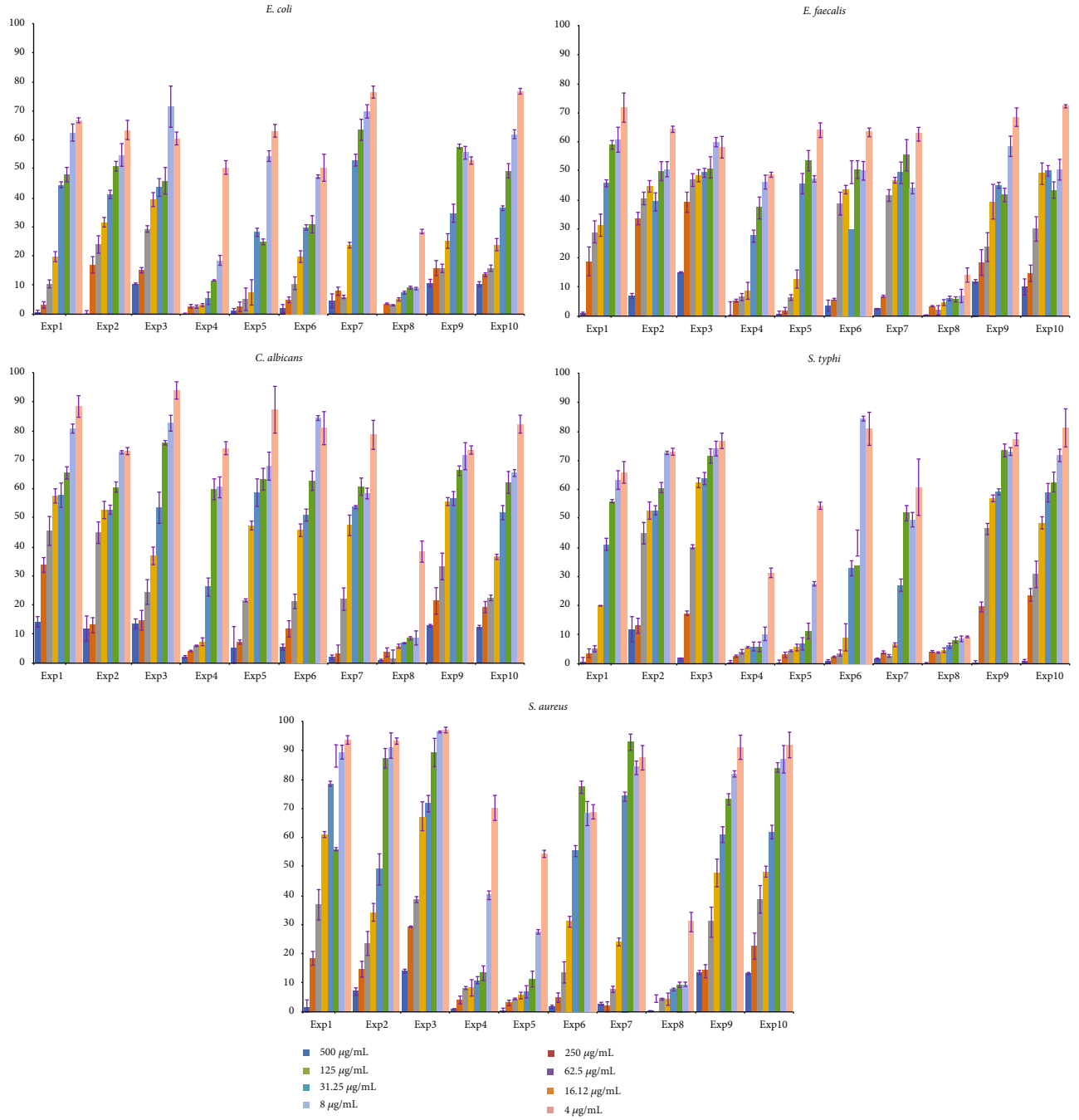

Figure 6: Viability percentage of five tested microorganism species, *E.coli*, *S. typhi*, *E. faecalis*, *S. aureus*, and *C. albicans*, treated by various concentrations of each as-prepared β-FeOOH nanorod based on the designed experiments (1–10).

samples (Figure 6). Our experiments were consistent with previous results of NR antimicrobial analysis. Ojha et al. reported that the lower aspect ratio of silver NRs exhibited significantly further antibacterial efficiency against both Gram-positive and Gram-negative bacterial species, comparing the aspect ratio of 1.8 and 3 [57].

More in detail, although the NRs obtained from Exp. 9 and 10 were synthesized in the presence of surfactant PEI, almost no antimicrobial effects of tested microorganisms with$\text{MIC} \geq 500\,\mu\text{g/mL}$ in all species were shown. It could be related to the larger size of NPs, which is a determining factor in the biological activities of nanomaterials. NRs synthesized in the presence of PEG (Exp. 4-7) provided an appropriately moderate susceptibility in all tested microbial species because of almost moderate particle size among synthesized NRs and appropriate aspect ratios, about 3-3.6.

C. albicans exhibited the least susceptibility to NRs with generally the most MIC value among all tested microbial species (Table 4). *C. albicans* is one of the opportunistic and pathogenic fungal species posing a particular challenge to the healthcare system due to their increasing drug resistance that should be addressed preferably [58]. Exp. 4

Table 4: MIC value of microbial strains treated with β-FeOOH nanorods obtained from the designed synthetic experiments, with and without the presence of surfactants.

Experiment	Surfactants (w/v)	S. typhi (μg/mL)	E. coli (μg/mL)	E. faecalis (μg/mL)	S. aureus (μg/mL)	C. albicans (μg/mL)
1	—	125	250	500	500	>500
2	—	250	500	500	500	>500
3	—	500	>500	>500	>500	>500
4	PEG-1%	16.12	31.25	62.5	62.5	62.5
5	PEG-3%	31.25	62.5	125	125	250
6	PEG-3%	62.5	250	250	250	500
7	PEG-6%	62.5	125	250	125	250
8	PEI-0.25%	4	8	8	8	8
9	PEI-0.5%	500	>500	>500	>500	>500
10	PEI-1.25%	500	>500	500	>500	>500

(PEG: 1% w/v, aspect ratio: 2.919) and Exp. 8 (PEI: 0.25% w/v, aspect ratio: 1.409) displayed high antifungal potentials with MIC values of 62.5 and 8 μg/mL, respectively, which could be considered as an antifungal agent in this case.

4. Conclusion

FeOOH NRs, especially in the β-phase, have attracted much attention in recent years to apply in biomedical applications. With the ever-increasing challenge of antimicrobial resistance, new innovative strategies are in high demand to combat. In the current study, ten synthesis experiments of β-FeOOH NRs are designed to optimize the NRs' properties toward the desirable antimicrobial potential. Reaction conditions, including reaction time and temperature and concentration of iron salt precursors, were considered essential in final particle characteristics and biological activities. Although these factors could affect particle size and aspect ratio, ferric ion concentration showed a dominant effect on the morphology of NRs. NRs also synthesized with and without the presence of surfactants of PEG and PEI, which could play good controlling roles in the size and growth pattern of NP crystals. The aspect ratio was also independent of all factors except ferric ion concentrations.

To sum up, our work indicated that synthetic conditions and the kind and concentration of surfactants contribute to the characterization properties and biological activities of final β-FeOOH NRs. Moreover, β-FeOOH NRs synthesized in the presence of surfactants exhibited more antimicrobial activities against Gram-positive and Gram-negative bacteria and fungi species, even though Gram-negative bacteria showed more susceptibility against NRs. Also, NRs synthesized in the presence of PEG generally revealed relatively moderate antimicrobial effects against tested bacterial and fungal species of final synthesized NPs compared to high antimicrobial activities of PEI surfactant. As mentioned above, surface active agents, particle size, and particularly aspect ratio are crucial decisive factors in the biological activities of β-FeOOH NRs as well as the concentration of NRs. Though further experimental investigations are required, the decent biocompatibility and antimicrobial efficacy of β-FeOOH NPs make them promising candidates for various biomedical applications.

Data Availability

All data used to support the findings of this study are included within the article.

Conflicts of Interest

The authors declare that there is no conflict of interest regarding the publication of this paper.

Authors' Contributions

Fatemeh Mohammadi and Salme Amiri contributed equally to this work.

Acknowledgments

This work was supported by the Shiraz University of Medical Sciences (grant number 25684).

References

[1] *10 global health issues to track in 2021*, World Health Organization, 2020, https://www.who.int/news-room/spotlight/10-global-health-issues-to-track-in-2021.

[2] N. E. Eleraky, A. Allam, S. B. Hassan, and M. M. Omar, "Nanomedicine fight against antibacterial resistance: an overview of the recent pharmaceutical innovations," *Pharmaceutics*, vol. 12, no. 2, p. 142, 2020.

[3] F. Fatima, S. Siddiqui, and W. A. Khan, "Nanoparticles as novel emerging therapeutic antibacterial agents in the antibiotics resistant era," *Biological Trace Element Research*, vol. 199, no. 7, pp. 2552–2564, 2021.

[4] S. Kumar, S. P. Pawar, K. Chatterjee, and S. Bose, "Antimicrobial and conducting polymer substrate derived from hybrid structures of silver nanoparticles and multiwall carbon nanotubes," *Materials Technology*, vol. 29, Supplement 1, pp. B59–B63, 2014.

[5] V. Agarwal and K. Chatterjee, "Recent advances in the field of transition metal dichalcogenides for biomedical applications," *Nanoscale*, vol. 10, no. 35, pp. 16365–16397, 2018.

[6] P. K. Samantaray, S. Indrakumar, K. Chatterjee, V. Agarwal, and S. Bose, "'Template-free' hierarchical MoS2foam as a sustainable 'green' scavenger of heavy metals and bacteria in point of use water purification," *Nanoscale Advances*, vol. 2, no. 7, pp. 2824–2834, 2020.

[7] F. Mohammadi, A. Gholami, N. Omidifar, A. Amini, S. Kianpour, and S.-M. Taghizadeh, "The potential of surface nano-engineering in characteristics of cobalt-based nanoparticles and biointerface interaction with prokaryotic and human cells," *Colloids and Surfaces. B, Biointerfaces*, vol. 215, p. 112485, 2022.

[8] S. M. Mousavi, S. A. Hashemi, A. Gholami et al., "Bioinorganic synthesis of polyrhodanine stabilized Fe3O4/graphene oxide in microbial supernatant media for anticancer and antibacterial applications," *Bioinorganic Chemistry and Applications*, vol. 2021, Article ID 9972664, 12 pages, 2021.

[9] S. R.-A. Narjes Ebrahimi, A. Ebrahiminezhad, Y. Ghasemi, A. Gholami, and H. Seradj, "Comparative study on characteristics and cytotoxicity of bifunctional magnetic-silver nanostructures: synthesized using three different reducing agents," *Acta Metallurgica Sinica*, vol. 29, no. 4, pp. 326–334, 2016.

[10] A. Gholami, S. Rasoul-amini, A. Ebrahiminezhad, S. H. Seradj, and Y. Ghasemi, "Lipoamino acid coated superparamagnetic iron oxide nanoparticles concentration and time dependently enhanced growth of human hepatocarcinoma cell line (HepG2)," *Journal of Nanomaterials*, vol. 2015, Article ID 451405, 9 pages, 2015.

[11] S. A. Hashemi, S. M. Mousavi, S. Bahrani et al., "Bio-enhanced polyrhodanine/graphene oxide/Fe_3O_4 nanocomposite with kombucha solvent supernatant as ultra-sensitive biosensor for detection of doxorubicin hydrochloride in biological fluids," *Materials Chemistry and Physics*, vol. 279, p. 125743, 2022.

[12] A. Gholami, S. M. Mousavi, S. A. Hashemi, Y. Ghasemi, W. H. Chiang, and N. Parvin, "Current trends in chemical modifications of magnetic nanoparticles for targeted drug delivery in cancer chemotherapy," *Drug Metabolism Reviews*, vol. 52, no. 1, pp. 205–224, 2020.

[13] S. M. Dadfar, D. Camozzi, M. Darguzyte et al., "Size-isolation of superparamagnetic iron oxide nanoparticles improves MRI, MPI and hyperthermia performance," *Journal of nanobiotechnology*, vol. 18, no. 1, p. 22, 2020.

[14] A. Gholami, F. Mohammadi, Y. Ghasemi, N. Omidifar, and A. Ebrahiminezhad, "Antibacterial activity of SPIONs versus ferrous and ferric ions under aerobic and anaerobic conditions: a preliminary mechanism study," *IET Nanobiotechnology*, vol. 14, no. 2, pp. 155–160, 2020.

[15] Z. Huang, F. Han, M. Li, Z. Zhou, X. Guan, and L. Guo, "Which phase of iron oxyhydroxides (FeOOH) is more competent in overall water splitting as a photocatalyst, goethite, akaganeite or lepidocrocite? A DFT-based investigation," *Computational Materials Science*, vol. 169, p. 109110, 2019.

[16] X. Wang, X. Chen, L. Gao et al., "Synthesis of β-FeOOH and α-Fe_2O_3nanorods and electrochemical properties of β-FeOOH," *Journal of Materials Chemistry*, vol. 14, no. 5, pp. 905–907, 2004.

[17] S.-M. Taghizadeh, A. Berenjian, M. Zare, and A. Ebrahiminezhad, "New perspectives on iron-based nanostructures," *Processes*, vol. 8, no. 9, p. 1128, 2020.

[18] G. Kasparis, A. S. Erdocio, J. M. Tuffnell, and N. T. K. Thanh, "Synthesis of size-tuneable β-FeOOH nanoellipsoids and a study of their morphological and compositional changes by reduction," *CrystEngComm*, vol. 21, no. 8, pp. 1293–1301, 2019.

[19] H. Cui, L. Wang, M. Shi, and Y. Li, "Morphology and phase control of iron oxide polymorph nanoparticles," *Materials Research Express*, vol. 4, no. 4, article 045006, 2017.

[20] X. Shi, L. Qin, G. Xu et al., "β-FeOOH: a new anode for potassium-ion batteries," *Chemical Communications*, vol. 56, no. 26, pp. 3713–3716, 2020.

[21] A. Berenjian, M. Karami-Darehnaranji, S.-M. Taghizadeh, E. Mirzaei, R. Heidari, and A. Ebrahiminezhad, "Bio-assisted synthesis of food-grade FeOOH nanoellipsoids as promising iron supplements for food fortification," *Applied Food Biotechnology*, vol. 8, no. 1, pp. 71–77, 2020.

[22] A. N. Fomenko, O. V. Bakina, S. O. Kazantsev, and A. M. Kondranova, "Synthesis of iron oxide based nanostructures with antimicrobial activity," *IOP Conf Ser Mater Sci Eng.*, vol. 447, article 012069, 2018.

[23] G. Yi, S. P. Teong, S. Liu, S. Chng, Y. Y. Yang, and Y. Zhang, "Iron-based nano-structured surfaces with antimicrobial properties," *Journal of Materials Chemistry B*, vol. 8, no. 44, pp. 10146–10153, 2020.

[24] D. T. N. Pham, F. Khan, T. T. V. Phan et al., "Biofilm inhibition, modulation of virulence and motility properties by FeOOH nanoparticle in Pseudomonas aeruginosa," *Brazilian Journal of Microbiology*, vol. 50, no. 3, pp. 791–805, 2019.

[25] Y. Wei, R. Ding, C. Zhang et al., "Facile synthesis of self-assembled ultrathin α-FeOOH nanorod/graphene oxide composites for supercapacitors," *Journal of Colloid and Interface Science*, vol. 504, pp. 593–602, 2017.

[26] Y. Piao, J. Kim, H. B. Na et al., "Wrap–bake–peel process for nanostructural transformation from β-FeOOH nanorods to biocompatible iron oxide nanocapsules," *Nature materials*, vol. 7, no. 3, pp. 242–247, 2008.

[27] R. M. Cornell and U. Schwertmann, *The Iron Oxides: Structure, Properties, Reactions, Occurrences and Uses*, John Wiley & Sons, 2003.

[28] M. Karami-Darehnaranji, S.-M. Taghizadeh, E. Mirzaei, A. Berenjian, and A. Ebrahiminezhad, "Size tuned synthesis of FeOOH nanorods toward self-assembled nanoarchitectonics," *Langmuir*, vol. 37, no. 1, pp. 115–123, 2021.

[29] J. Yue, X. Jiang, and A. Yu, "Experimental and theoretical study on the β-FeOOH nanorods: growth and conversion," *Journal of Nanoparticle Research*, vol. 13, no. 9, pp. 3961–3974, 2011.

[30] F. N. Sayed and V. Polshettiwar, "Facile and sustainable synthesis of shaped iron oxide nanoparticles: effect of iron precursor salts on the shapes of iron oxides," *Scientific Reports*, vol. 5, no. 1, p. 9733, 2015.

[31] H. Moradpoor, M. Safaei, F. Rezaei et al., "Optimisation of cobalt oxide nanoparticles synthesis as bactericidal agents," *Open access Macedonian journal of medical sciences*, vol. 7, no. 17, pp. 2757–2762, 2019.

[32] T. Zhu, J. S. Chen, and X. W. Lou, "Glucose-assisted one-pot synthesis of FeOOH nanorods and their transformation to Fe_3O_4@ carbon nanorods for application in lithium ion batteries," *Journal of Physical Chemistry C*, vol. 115, no. 19, pp. 9814–9820, 2011.

[33] K. Chen, X. Chen, and D. Xue, "Hydrothermal route to crystallization of FeOOH nanorods via $FeCl_3{\cdot}6H_2O$: effect of Fe^{3+} concentration on pseudocapacitance of iron-based materials," *CrystEngComm*, vol. 17, no. 9, pp. 1906–1910, 2015.

[34] X. Wei, X. Mou, Y. Zhou, Y. Li, and W. Shen, "Fabrication of rod-shaped β-FeOOH: the roles of polyethylene glycol and chlorine anion," *Science China Chemistry*, vol. 59, no. 7, pp. 895–902, 2016.

[35] J. Zhang, X. Zhu, and K. Yu, "Surfactant-assisted nanorod synthesis of α-FeOOH and its adsorption characteristics for methylene blue," *Journal of Materials Research*, vol. 29, no. 4, pp. 509–518, 2014.

[36] Y. Zhou, W. Wu, G. Hu, H. Wu, and S. Cui, "Hydrothermal synthesis of ZnO nanorod arrays with the addition of polyethyleneimine," *Materials Research Bulletin*, vol. 43, no. 8-9, pp. 2113–2118, 2008.

[37] J. Mohapatra, A. Mitra, H. Tyagi, D. Bahadur, and M. Aslam, "Iron oxide nanorods as high-performance magnetic resonance imaging contrast agents," *Nanoscale*, vol. 7, no. 20, pp. 9174–9184, 2015.

[38] R. Parameshwari, P. Priyadarshini, and G. Chandrasekaran, "Optimization, structural, spectroscopic and magnetic studies on stable akaganeite nanoparticles via co-precipitation method," *American Journal of Materials Science*, vol. 1, no. 1, pp. 18–25, 2011.

[39] E. Murad and J. L. Bishop, "The infrared spectrum of synthetic akaganéite, β-FeOOH," *American Mineralogist*, vol. 85, no. 5-6, pp. 716–721, 2000.

[40] S. M. Pasini, M. A. Batistella, S. M. A. G. U. de Souza, J. Wang, D. Hotza, and A. A. U. de Souza, "Thermal degradation and flammability of TiO_2–polyetherimide nanocomposite fibers," *Polymer Bulletin*, vol. 77, no. 9, pp. 4937–4958, 2020.

[41] S. Arabi, H. Akbari Javar, and M. Khoobi, "Preparation and characterization of modified polyethyleneimine magnetic nanoparticles for cancer drug delivery," *Journal of Nanomaterials*, vol. 2016, Article ID 2806407, 6 pages, 2016.

[42] S. K. Seol, D. Kim, S. Jung, W. S. Chang, and J. T. Kim, "One-step synthesis of PEG-coated gold nanoparticles by rapid microwave heating," *Journal of Nanomaterials*, vol. 2013, Article ID 531760, 6 pages, 2013.

[43] J. Charmi, H. Nosrati, J. Mostafavi Amjad, R. Mohammadkhani, and H. Danafar, "Polyethylene glycol (PEG) decorated graphene oxide nanosheets for controlled release curcumin delivery," *Heliyon*, vol. 5, no. 4, article e01466, 2019.

[44] H. Ahmad, K. Umar, S. Ali, P. Singh, S. Islam, and H. Khan, "Preconcentration and speciation of arsenic by using a graphene oxide nanoconstruct functionalized with a hyperbranched polyethyleneimine," *Mikrochimica Acta*, vol. 185, no. 6, 2018.

[45] R. Wang, L. Wu, D. Zhuo, Z. Wang, and T. Y. Tsai, "Fabrication of fullerene anchored reduced graphene oxide hybrids and their synergistic reinforcement on the flame retardancy of epoxy resin," *Nanoscale Research Letters*, vol. 13, no. 1, p. 351, 2018.

[46] K. Grenda, A. Idström, L. Evenäs, M. Persson, K. Holmberg, and R. Bordes, "An analytical approach to elucidate the architecture of polyethyleneimines," *Journal of Applied Polymer Science*, vol. 139, no. 7, p. 51657, 2022.

[47] X. Zhang, L. An, J. Yin, P. Xi, Z. Zheng, and Y. Du, "Effective construction of high-quality iron oxy-hydroxides and Co-doped iron oxy-hydroxides nanostructures: towards the promising oxygen evolution reaction application," *Scientific Reports*, vol. 7, no. 1, pp. 1–10, 2017.

[48] N. K. Chaudhari and J.-S. Yu, "Size control synthesis of uniform β-FeOOH to high coercive field porous magnetic α-Fe_2O_3 nanorods," *Journal of Physical Chemistry C*, vol. 112, no. 50, pp. 19957–19962, 2008.

[49] M. Nabavizadeh, A. Abbaszadegan, A. Gholami et al., "*Antibiofilm efficacy of positively charged imidazolium-based silver nanoparticles in Enterococcus faecalis using quantitative real-time PCR*," *Jundishapur Journal of Microbiology*, vol. 10, no. 10, article e55616, 2017.

[50] A. Abbaszadegan, M. Nabavizadeh, A. Gholami et al., "Positively charged imidazolium-based ionic liquid-protected silver nanoparticles: a promising disinfectant in root canal treatment," *International Endodontic Journal*, vol. 48, no. 8, pp. 790–800, 2015.

[51] F. D. Lowy, "Antimicrobial resistance: the example of Staphylococcus aureus," *The Journal of Clinical Investigation*, vol. 111, no. 9, pp. 1265–1273, 2003.

[52] L. Peng, L. Chang, X. Liu et al., "Antibacterial property of a polyethylene glycol-grafted dental material," *ACS Applied Materials & Interfaces*, vol. 9, no. 21, pp. 17688–17692, 2017.

[53] W. Akhtar, M. Shoaib, I. M. Khan et al., "Improved bactericidal activity of polyethylenimine grafted graphene oxide nanocomposite against Staphylococcus aureus and Escherichia coli," *Biomedical Journal of Scientific & Technical Research*, vol. 27, no. 2, pp. 20616–20624, 2020.

[54] H. Shi, H. Liu, S. Luan et al., "Effect of polyethylene glycol on the antibacterial properties of polyurethane/carbon nanotube electrospun nanofibers," *RSC Advances*, vol. 6, no. 23, pp. 19238–19244, 2016.

[55] D. Kilinc, C. L. Dennis, and G. U. Lee, "Bio-Nano-magnetic materials for localized mechanochemical stimulation of cell growth and death," *Advanced Materials*, vol. 28, no. 27, pp. 5672–5680, 2016.

[56] S. Dasgupta, T. Auth, and G. Gompper, "Shape and orientation matter for the cellular uptake of nonspherical particles," *Nano Letters*, vol. 14, no. 2, pp. 687–693, 2014.

[57] A. K. Ojha, S. Forster, S. Kumar, S. Vats, S. Negi, and I. Fischer, "Synthesis of well–dispersed silver nanorods of different aspect ratios and their antimicrobial properties against gram positive and negative bacterial strains," *Journal of nanobiotechnology*, vol. 11, no. 1, p. 42, 2013.

[58] H. A. P. Castillo, L. N. M. Castellanos, R. M. Chamorro, R. R. Martínez, and E. O. Borunda, *Nanoparticles as New Therapeutic Agents against Candida albicans*, Candida Albicans, Doblin Sandai, IntechOpen, 2018.